of traps. Work is in progress to evaluate the capacitance associated with the device to optimize the frequency behavior.

CONCLUSION

An analytical model for a pseudomorphic MODFET is presented to evaluate its output characteristics. It is shown that the AlGaAs/InGaAs MODFET has better charge control and higher transconductance than the AlGaAs/GaAs MODFET. We attribute these improvements to the larger effective conduction band discontinuity, improved confinement of electrons in the InGaAs channel, and the better transport properties in the AlGaAs/InGaAs system. The present model is highly suitable for MMIC design as it determines the electrical and microwave performance of the device.

REFERENCES

1. H. Morkoc and P.M. Solomon, The HEMT: A superfast transistor, IEEE Spectrum 21 (1984), 28–35.
2. S. Sen, M.K. Pandey, and R.S. Gupta, A two dimensional I-V model for frequency optimization of heterostructure field effect transistor, Proc Int Conf Comput and Devices for Commun (CODEC-98), Calcutta, India, 1998, pp. 388–390.
3. S. Sen, M.K. Pandey, and R.S. Gupta, Bandgap discontinuity model for 2DEG density at the AlGaAs/GaAs interface, Proc Asia-Pacific Microwave Conf, 1996, pp. 243–246.
4. T.E. Zipperian, L.R. Dawson, G.C. Osbourn, and I.J. Fritz, An $In_{.2}Ga_{.8}As$/GaAs modulation doped strained layer superlattice field effect transistor, IEDM Tech Dig, 1983, pp. 696–699.
5. J.J. Rosenberg, M. Benlamri, P.D. Kirchner, J.M. Woodall, and J.P. Pettit, Pseudomorphic InGaAs/GaAs single quantum well high electron mobility transistor, IEEE Electron Device Lett EDL-6 (1985), 491–493.
6. T.E. Zipperian and T.J. Drummond, Strained quantum-well, modulation doped field effect transistor, Electron Lett 21 (1985), 823–824.
7. N. Chand, T. Henderson, J. Klem, W.T. Masselink, R. Fischer, Y.C. Chang, and H. Morkoc, Comprehensive analysis of Si doped $Al_xGa_{1-x}As$ ($x = 0$ to 1): Theory and experiments, Phys Rev B 30 (1984), 4481–4492.
8. D. Delageleaudeuf and N.T. Linh, Metal-(n) AlGaAs/GaAs two dimensional electron gas FET, IEEE Trans Electron Devices ED-29 (1982), 955–960.
9. Y.H. Byun, Unified charge control model and subthreshold current in heterostructure field effect transistors, IEEE Electron Device Lett 11 (1990), 50–53.
10. M.L. Majewski, An analytical DC model for the modulation doped field effect transistor, IEEE Trans Electron Devices ED-34 (1987), 1902–1909.
11. K.-W. Liu and A.F.M. Anwar, A self consistent calculation of the small signal parameters for AlGaAs/GaAs and AlGaAs/InGaAs/GaAs HEMTs, Solid State Electron 37 (1994), 51–54.
12. A.A. Ketterson, W.T. Masselink, J.S. Gedymin, J. Klem, C.K. Peng, W.F. Kopp, H. Morkoc, and K.R. Gleason, Characterization of InGaAs/AlGaAs pseudomorphic modulation doped field effect transistor, IEEE Trans Electron Devices ED-33 (1986), 564–571.

MEASUREMENT OF ELECTRICALLY TUNABLE LIQUID-CRYSTAL FABRY–PEROT INTERFEROMETER USING A MONOCHROMATIC LIGHT SOURCE

Kuen-Cherng Lin,[1] Jin-Shin Lin,[2] Po-Lun Chen,[3] and Wei-Ching Chuang[4]
[1] Department of Electrical Engineering
Kuang-Wu Institute of Technology and Commerce
Taipei, Taiwan, R.O.C.
[2] Department of Electronics
Van-Unng Institute of Technology
Taoyuan, Taiwan, R.O.C.
[3] Institute of Electro-Optics
National Chiao-Tung University
Hsin-Chu, Taiwan, R.O.C.
[4] Department of Electro-Optics
National Huwei Institute of Technology
Yunlin, Taiwan, R.O.C.

Received 4 January 1999

ABSTRACT: *We propose a novel technique to characterize an electrically tunable liquid-crystal Fabry–Perot interferometer. Only one usual set of a monochromatic light source and an optical power meter is needed. Various characteristic parameters were estimated based on the equivalent refractive index analysis and the measured voltage-dependent transmittance.* © 1999 John Wiley & Sons, Inc. Microwave Opt Technol Lett 22: 48–51, 1999.

Key words: *Fabry–Perot interferometer; monochromatic light source; optical measurements*

1. INTRODUCTION

Tunable wavelength filters have found numerous applications [1–3] in optical tuners, tunable lasers, wavelength-conversion lasers, and tunable demultiplexers. The liquid-crystal Fabry–Perot interferometer (LC–FPI) has clear advantages over other types of wavelength-selective filters [2] due to its simple structure, low loss, low-voltage driving, narrow bandwidth, and wide tunable range. By applying a voltage of 1–5 V to change the refractive index of liquid crystal, and hence the optical path length in the cavity of the Fabry–Perot etalon, an electrically tunable LC–FPI filter can be widely tuned. Performance measurement and assessment of an optical filter are very important in practical designs and applications in optical systems. Currently, a broad-spectrum CW light source, or a number of monochromatic lasers, as well as an optical spectrum analyzer with a resolution below 0.1 nm are used to measure such an LC–FPI [4–5]. This straightforward concept of measurement is also widely applied to the other kinds of optical filters.

In this letter, we propose a novel technique to characterize an electrically tunable LC–FPI, in which only the usual set of the combination of a monochromatic light source and an optical power meter is needed. It is based on the equivalent refractive index (ERI) analysis of a liquid-crystal Fabry–Perot etalon [6]. The cavity length and FWHM (full width at half maximum) were estimated according to the voltage-dependent transmittance function. Good agreement between the experimental measurement and theoretical simulation indicates the validity of the proposed technique.

2. MEASUREMENT SETUP

Figure 1 shows a schematic diagram of the experimental setup to measure an LC–FPI filter. An He–Ne laser with a wavelength of $\lambda_0 = 0.6328$ μm is used as a monochromatic light source. A voltage signal is applied to the LC–FPI filter to tune light transmission or, equivalently, to control the center wavelength of the output light beam if the light source is replaced by a broad-spectrum CW laser. The applied signal is ac (1 kHz, $V_{\rm rms} = 0$–7.5 V) to prevent the screening of applied field caused by the impurity ions in LC. A polarizer is used to assure the polarization of the input light parallel to the director of the LC cavity. Since LC molecules change their orientation subject to an applied field, the refractive index and transmission experienced by the linearly polarized light beam vary. The output power is measured by an ordinary optical power meter. Thus, the voltage-dependent transmittance functions can be obtained using an oscilloscope. Typical results are shown in Figure 2. In these cases, the liquid crystal cells of the LC–FPI were injected with the nematic LC (Merck ZLI–3103, $n_o = 1.4771$, $n_e = 1.5506$) and spaced with 15 and 8 μm spacers, respectively.

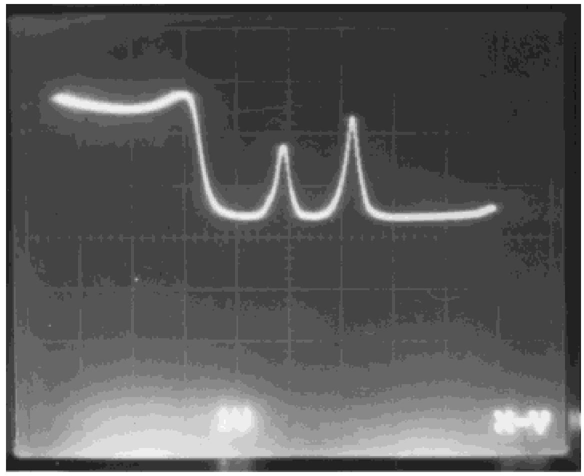

(a)

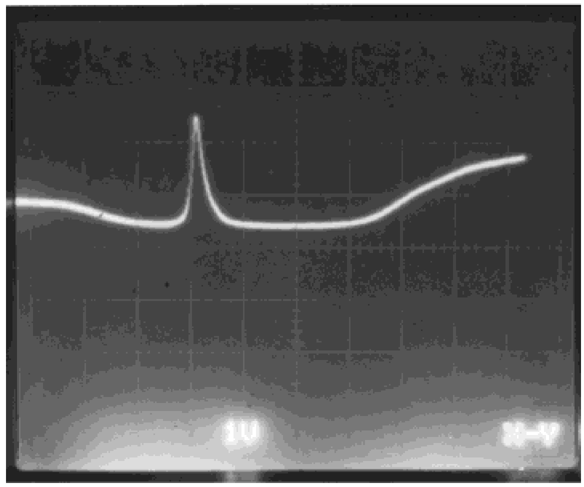

(b)

Figure 2 Photographs of the experimental results on the dependence of the transmittance by "intensity measurement" which is shown on an oscilloscope with detector signals in the y-axis and tuning voltage in the x-axis. The LC cells have (a) 15 μm and (b) 8 μm spacers

3. RESULTS AND DISCUSSION

Plots of the voltage-dependent transmittance, including both theoretical calculation and experimental measured values corresponding to Figure 2, are given in Figure 3. The small discrepancy can come from the fact that the LC molecules close to the alignment surface do not reorient even though the applied voltage is sufficient. From this figure, it is convenient for us to estimate the cavity length of an LC–FPI filter as well as the FWHM of the filter, based on the voltage-dependent equivalent refractive index by ERI analysis [6]. The cavity length is a basic parameter to evaluate the resonance wavelengths, and hence the free spectral range (FSR) and tunable range. It can be derived as

$$d = \frac{\lambda}{2} \cdot \frac{1}{n_{r1} - n_{r2}} = \frac{\lambda}{2} \cdot \frac{1}{n(V_{r1}) - n(V_{r2})} \qquad (1)$$

where V_{r1} and V_{r2} are the required voltage for two adjacent resonance peaks, which correspond to the required refractive indexes n_{r1} and n_{r2}, respectively. Considering a sample with an LC cell spaced by the 15 μm spacer [Fig. 2(a)], two adjacent peaks in the transmittance curve are present at $V_{r1} = 2.9$ V and $V_{r2} = 4.3$ V, corresponding to $n_{r1} = 1.5281$

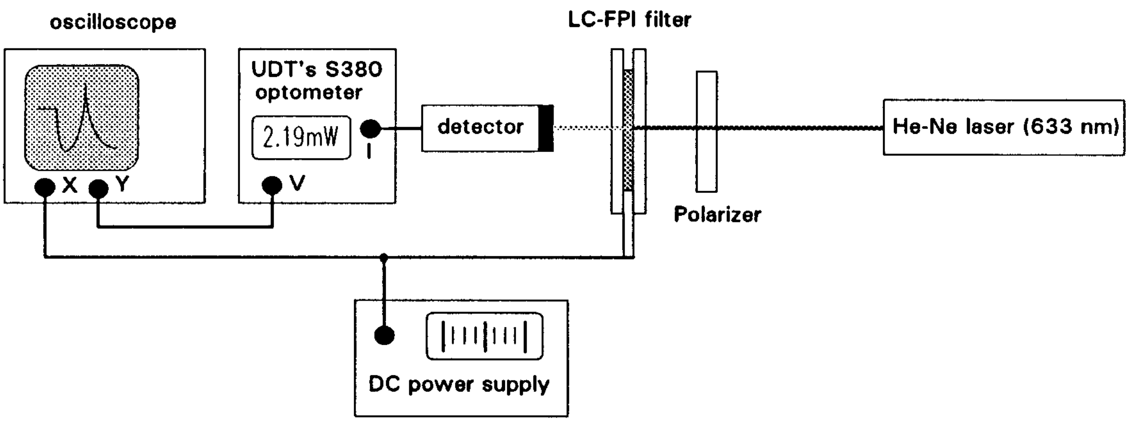

Figure 1 Setup for the "intensity measurement" experiment

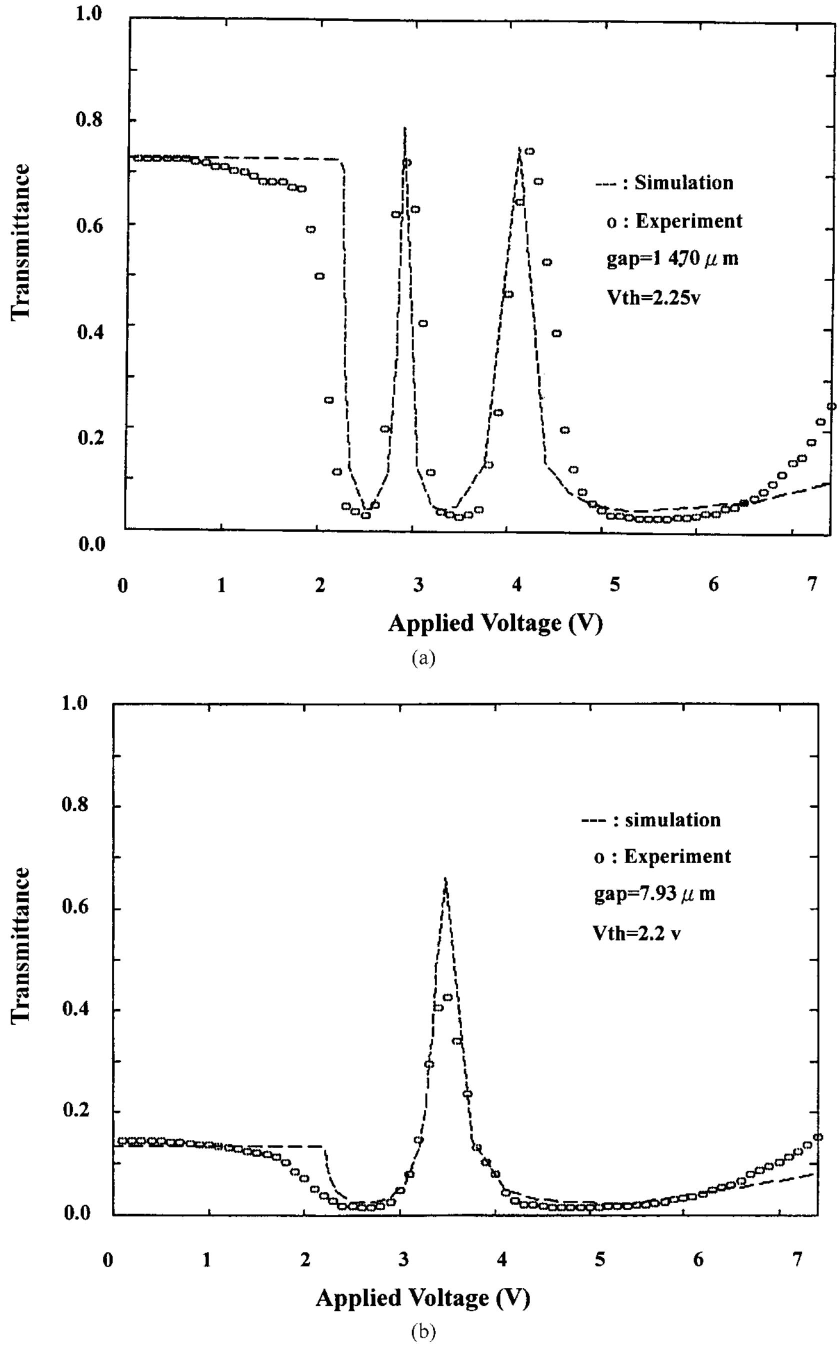

(a)

(b)

Figure 3 Simulated and experimental results on the dependence of the transmittance by "intensity measurement" for different LC cells with (a) 15 μm, and (b) 8 μm spacers

and $n_{r2} = 1.5063$, respectively. Thus, the cavity gap was estimated to be 14.57 μm.

It is easily understood that the full voltage width at the half maximum in voltage-dependent transmittance characteristics corresponds to the full bandwidth at the half maximum in the wavelength-dependent transmittance characteristics. To obtain the FWHM of a passband centered at wavelength λ_0, the wavelengths at the half maximum of the transmittance λ_1 and λ_2 have to be measured. That is, a voltage V_0 induces an equivalent refractive index $n_0 = n_{\text{equ}}(V_0)$, in which the effective cavity gap for resonance is equal to $n_0 \cdot L$, such that light at a wavelength λ_0 passes through the LC–FPI filter at maximum. On the other hand, when V_1 is applied, $n_1 = n_{\text{equ}}(V_1)$, where the effective cavity gap equals $n_1 \cdot L$, and hence, only a half maximum of transmittance at λ_1 would pass through the filter. The relationship between V_2 and n_2 at λ_2 is similar to the λ_1 case.

The FWHM is mathematically expressed as FWHM $= \lambda_1 - \lambda_2$, where λ_1 and λ_2 correspond to the refractive indexes n_1 and n_2 as well as the applied voltages V_1 and V_2, respectively. Thus, the FWHM becomes

$$\mathrm{FWHM} = \lambda(n_1) - \lambda(n_2) = \lambda(n(V_1)) - \lambda(n(V_2)) \quad (2)$$

where V_1 and V_2 can be obtained from the above measurement. We thus have

$$\mathrm{FWHM} = \lambda_1 - \lambda_2 = 2(\lambda_2 - \lambda_0) = 2\lambda_0\left(\frac{n_2}{n_0} - 1\right) \quad (3)$$

due to the fact that $(2\pi n_0/\lambda_0) = (2\pi n_1/\lambda_1) = (2\pi n_2/\lambda_2) = m\pi$ at the same resonance order m.

For the case of an 8 μm spacer [Fig. 2(b)], we get $V_0 = 3.62$ V and $V_2 = 3.48$ V, which give $n_0 = 1.5129$ and $n_2 = 1.5152$, respectively. The variation of n_{equ} with respect to the external electric voltage is on the order of magnitude of 10^{-3}. Substituting these data into the above equation, we estimate the FWHM to be 1.92 nm; yet, that which was given by an optical spectrum analyzer is 1.96 nm. The accuracy of FWHM estimation is strongly influenced by both the stability of the externally applied voltage and the coupling ratio. Because the FWHM estimation focuses on the much smaller region calculation in the transmittance curve, it naturally requires a much more strict experimental condition.

4. CONCLUSIONS

A novel technique to characterize an electrically tunable LC–FPI was presented. Only the usual set of a monochromatic light source and an optical power meter is needed. It is based on the equivalent-refractive-index analysis of a liquid-crystal Fabry–Perot etalon. Estimation of the cavity length and FWHM was achieved according to the measured voltage-dependent transmittance function.

REFERENCES

1. Y. Suzuki, N. Ohta, and K. Hirabayashi, Nonlinear distortion due to Fabry–Perot optical filter in direct modulated dense WDM-SCM viedo distribution systems, IEEE Photon Technol Lett 4 (1993), 466–468.
2. K. Hirabayashi, H. Tsuda, and T. Kurokawa, Tunable liquid-crystal Fabry–Perot interferometer filter for wavelength-division multiplexing communication systems, J Lightwave Technol 5 (1993), 2033–2043.
3. H. Tsuda, H. Uenohara, H. Iwamura, K. Hirabayashi, and T. Kurokawa, Tunable wavelength conversion using a liquid crystal filter and a bistable laser diode, Appl Phys Lett 61 (1992), 2006–2008.
4. M.W. Maeda, J.S. Patel, L. Chinlon, J. Horrobin, and R. Spicer, Electrically tunable liquid-crystal etalon filter for high-density WDM system, IEEE Photon Technol Lett 2 (1990), 820–822.
5. J.S. Patch, M.A. Saifi, D.W. Berreman, L. Chinlon, N. Andreadakis, and S.D. Lee, Electrically tunable optical filter for infrared wavelength using liquid crystal in a Fabry–Perot etalon, Appl Phys Lett 57 (1990), 1718–1719.
6. P.-L. Chen, K.-C. Lin, W.-C. Chuang, Y.-C. Tzent, K.-Y Lee, and W.-Y. Lee, Analysis of a liquid crystal Fabry–Perot etalon filter: A novel model, IEEE Photon Technol Lett 9 (1997), 467–469.

CCC 0895-2477/99

MILLIMETER-WAVE ARRAY FED THROUGH THICK SLOTS FILLED WITH DIELECTRIC

M. El Haj Sleimen,[1] M. Himdi,[1] J. P. Daniel,[1] N. Haese,[2] and P. A. Rolland[2]

[1] UPRES-A CNRS 6075 Structure Rayonnantes/Antennes et Réseaux
Université de Rennes I
35042 Rennes, France
[2] Département Hyperfréquences et Semiconducteurs
IEMN UMR CNRS 9929
59652 Villeneuve d'Ascq Cedex, France

Received 5 January 1999

ABSTRACT: *This paper deals with millimeter-wave microstrip antenna arrays. The objectives were to develop and optimize a microstrip-to-thick-slot-line transition near 40 GHz, and to feed a printed array with this kind of transition. The influence of such a transition between the two layers, and its effect on the radiation properties (pattern symmetry, sidelobe level) have been checked. A study of the microstrip / thick-slot / microstrip transition is first presented. Then, a comparison is made between radiated fields of arrays fed directly and through slot transitions.* © 1999 John Wiley & Sons, Inc. Microwave Opt Technol Lett 22: 51–53, 1999.

Key words: *millimeter wave; thick slot; transition; radiation patterns*

1. INTRODUCTION

The development of civil applications in the millimeter-wave domain already requires the realization of antenna arrays in this frequency band. Microstrip technology is attractive at these frequencies if one uses materials with weak losses and cost.

But a problem often appears in the millimeter-wave domain; spurious radiations, owing to the feeding network, occur. They are combined with the wanted radiation of the array which is degraded. These effects will affect the cross-polarization component and the sidelobe levels of the copolarization component.

A means to palliate this problem is to print the array on two distinct faces: the radiating elements on one face, and the feeding network, responsible for the parasitic radiation, on the other. To join the two faces of the circuit, various options are foreseeable. Among them are the microstrip-to-coaxial transition [1], and the microstrip-to-thick-slot transition. The latter solution is chosen in this paper.

We will begin with a study of this transition. Then we will use it to feed a printed array, and will observe the effects of this association on the radio electrical behavior of the array.

2. MICROSTRIP-TO-THICK-SLOT TRANSITION IN MILLIMETER-WAVE DOMAIN

2.1. Description of the Transition. The structure is composed of a thick slot filled with dielectric that couples two microstrip lines printed on different layers (Fig. 1).

The dielectric used here is a polymer, homogeneous, low-cost, and well suited for microwaves material: the polymethyl–pentene alias TPX [2]. In the range of 39 GHz, its thickness (h) equals 254 μm. It presents the following dielectric characteristics: $\varepsilon_r = 2.1$ and $\tan(\delta) = 10^{-3}$. The metalization is copper with 17.5 μm thickness (t).

The thick support in which the slot is engraved is copper or other plated material of H_s thickness.